46th Annual Review of Progress in Quantitative Nondestructive Evaluation
QNDE2019
July 14-19, 2019, Portland, OR, USA

QNDE2019-

ADVANCED BOREHOLE REFLECTION IMAGNG AND APPLIATIONS

Xiaoming Tang[1]
School of Geosciences, China University of Petroleum, Qingdao 266580, China

ABSTRACT

Borehole acoustic reflection imaging has recently emerged as an important geophysical well-logging technology in hydrocarbon exploration. This technology greatly enhances the ability to image reservoir structures away from borehole. This presentation provides an overview on the advancement of this technology and its applications. The most significant advance is shear-wave reflection imaging using borehole dipole sources, whose directional aspect allows for determining striking azimuth of a geological structure. The azimuthal sensitivity of the dipole shear-wave imaging has been validated by a repeatability test using two logging runs with different orientations, and by comparing the imaging result with available borehole-wall resistivity images. This technology has also been applied to field dipole logging measurements in deviated and horizontal wells. The result shows that it can image bedding planes above and below the well, and detect vertical fractures near the well.

Keywords: shear wave, reflection imaging, azimuth sensitivity, deviated well

1. INTRODUCTION

Single-well acoustic reflection imaging uses an acoustic source-receiver system in a borehole to radiate and receive elastic waves to and from a remote geologic reflector in formation, allowing for imaging geological features away from borehole. The imaging can use compressional (P) and shear (S) waves from a logging tool. Early techniques primarily use P waves from a monopole tool[1,2,3]. Later developments use S waves from a dipole tool[4,5,6,7]. A dipole source can radiate *SV*- and *SH*-types of shear waves into formation. Theoretical analyses[7,8,9,10] show that the SH wave dominates the radiated elastic wavefield and has broad angular coverage compared to the *SV* wave, especially for high-angle reflectors. The dipole-shear wave, compared to the monopole P wave, has lower frequency content and can thus penetrate deeper into formation. Besides, the azimuthal sensitivity of the dipole shear wave allows for determining the strike azimuth of a reflector. Further, for imaging fractures that have a sharp shear rigidity discontinuity, the shear wave, being sensitive to formation shear rigidity, can sense fractures better than P waves. Because of these advantages, dipole-shear wave imaging has been rapidly developing in recent years. However, a drawback of dipole S-wave imaging is the 180° ambiguity. This means the dipole S-imaging can determine the striking, but not the dipping, direction of a reflector.

2. METHOD AND VALIDATION

2.1 Method

This study focuses primarily on the advantage of using the azimuthal sensitivity of the dipole shear-wave imaging. The dipole acoustic source–receiver system radiates and receives shear waves to and from remote geologic reflectors in the formation, allowing for imaging geological features, such as fractures, faults, bed boundaries, etc. Compared to the reflected P-wave imaging with a monopole, the particular advantage for the dipole-shear imaging is that, by combing the four-component (4C) data of the cross-dipole system, the strike azimuth of the geological reflector can be determined. The 4C data set consists of *xx*, *xy*, *yx*, and *yy* components, where the first (second) letter refers to the source (receiver) orientation, which form a 2×2 symmetric matrix that can be used to generate a new 4C data *XX*, *XY*, *YX*, and *YY* for any given azimuthal direction using the coordinate transformation or matrix rotation[6]

$$\begin{pmatrix} XX & XY \\ YX & YY \end{pmatrix} = \begin{pmatrix} \cos AZ & \sin AZ \\ -\sin AZ & \cos AZ \end{pmatrix} \begin{pmatrix} xx & xy \\ yx & yy \end{pmatrix} \begin{pmatrix} \cos AZ & -\sin AZ \\ \sin AZ & \cos AZ \end{pmatrix} \quad (1)$$

where *AZ* is the angle between the *X*-axis of the new coordinates and the *x*-axis of the tool-frame coordinates. Thus, by varying the azimuth *AZ* to diagonalize the rotated matrix, the true reflector strike azimuth *AZ* can be determined. However, due to the symmetry of the data matrix, the rotation analysis only obtains the strike direction of the reflector.

[1] Xiaoming Tang: tangxiam@aliyun.com

© 2019 by ASME

2.2 Validation using repeatability test

To validate the azimuthal sensitivity of borehole dipole shear-wave reflection imaging, a repeatability test was carried out for a 60m borehole section along a fractured formation. This well was logged twice with a 4C cross-dipole tool. The tool orientation for the two logging runs was very different. Panel 1 of Figure 1 shows the tool azimuth log curves for the two runs, labeled as Run 1 (red) and Run 2 (black), respectively. Despite the drastically different tool orientations, the shear-wave images obtained from the two data sets are quite similar. Panels 2 and 3 show the imaging result for Run 1 and Run 2, respectively. By applying equation (1) to the data, a high angle fracture is best imaged at the NNE azimuth for both Run 1 and Run 2, as indicated by the arrows in each panel. This repeatability test demonstrates the azimuthal aspect of the dipole shear-wave imaging. That is, by recording the 4C reflection data, the dipole shear-wave imaging can determine the strike azimuth of a geological reflector regardless of the tool orientation during logging.

2.3 Validation by comparing with borehole-wall image

In the processing example of Figure 2, equation (1) was applied to the 4C cross-dipole data from another fractured formation. By varying the azimuth AZ to diagonalize the rotated data matrix of equation (1), the images from two diagonal terms of the matrix correspond to the shear-wave images along the NS (panel 1) and EW (panel 2) strike directions, respectively. In a radial depth range about 20m around the well, the EW image shows many vertical features, while the NS image shows very few features except some near-borehole stripes corresponding to the residuals from direct borehole wave suppression. To verify the features on the EW image, the borehole-wall resistivity image (right panel) is displayed for the depth interval indicated by two arrows. The resistivity image shows a vertical fracture crossing the borehole approximately in the EW direction. This shows that the features on the dipole shear-wave image of panel 2 are the vertical formation fractures striking along the EW azimuth. However, due to the 180° ambiguity of the dipole data, the imaged fractures appear symmetric around the borehole. Further research work is needed to resolve this ambiguity.

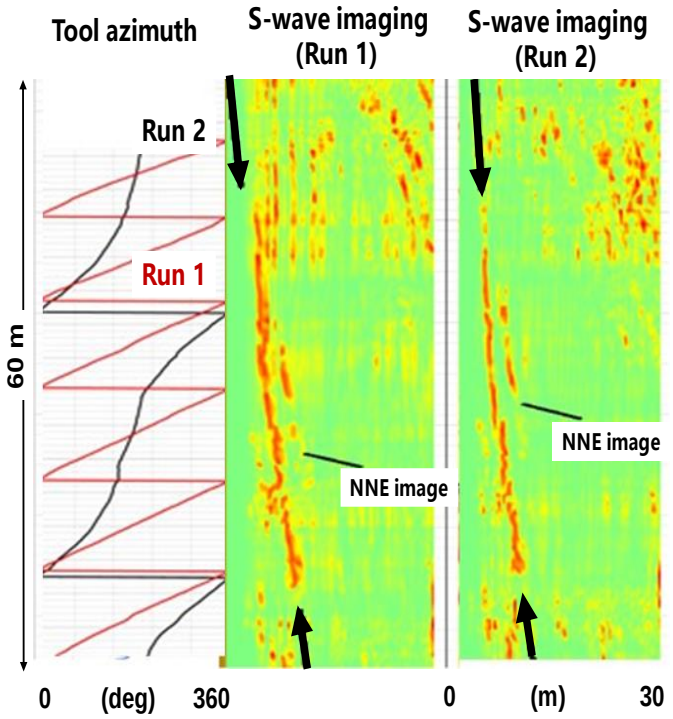

FIGURE 1: DIPOLE SHEAR-WAVE REFLECTION IMAGES (PANELS 2 AND 3) FROM A REPEATABILITY TEST WITH DIFFERENT TOOL ORIENTATIONS (PANEL 1)

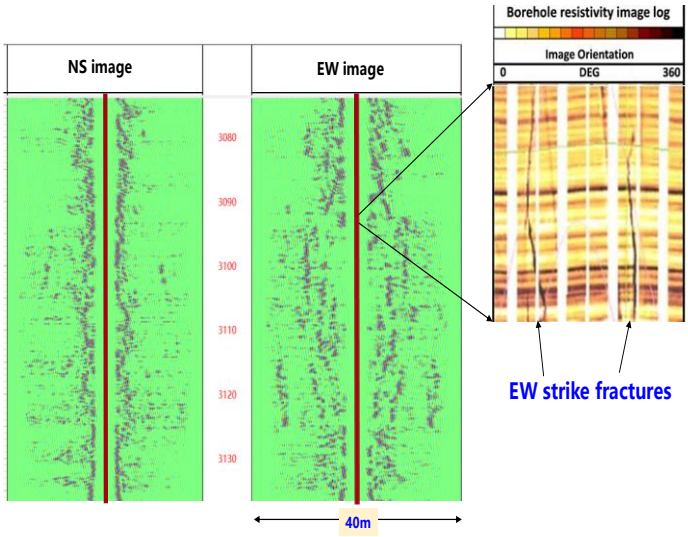

FIGURE 2: DIPOLE SHEAR-WAVE REFLECTION IMAGING FOR THE NS (PANEL1) AND EW (PANEL 2) AZIMUTHS. THE RESISTIVITY IMAGE (PANLE 3) CONFIRMS THAT THE FEATURES ON THE EW IMAGE ARE EW-STRIKING VERTICAL FRACTURES

© 2019 by ASME

3. APPLICATION TO HIGH-ANGLE WELLS

The rotational analysis of equation (1) can be applied to the 4C cross-dipole data acquired in high-angle and/or deviated wells. Note in the rotation analysis using equation (1), the tool azimuth curve relative to the borehole high side is used. The 4C data set is rotated into the *SH* and *SV* shear waves. The *SH* wave polarizes in the horizontal plane, and the *SV* wave polarizes in the vertical plane. The horizontally polarized *SH* wave is best suited for imaging horizontal reflectors (e.g., bedding planes) above and below the well. The *SV* wave, because its polarization is in the vertical plane, is best suited for imaging vertical features (e.g., fractures) on each side of the borehole.

The field data example in Figure 3 is used to demonstrate the application. As the borehole deviation curve (*DEV*, panel 1 of Figure 3(a)) shows, in a 160m section along the well, the borehole starts from a deviation of 60° and lands to horizontal at the end of the section. The formation lithology encountered during this landing process shows significant changes (see the gamma-ray (*GR*) curve in panel 1). The image from the horizontally polarized *SH* wave is displayed in panel 2 of Figure 3(a), in a radial distance range about 23m above and below the well. The image shows numerous bedding planes crossing the well. Because of the varying borehole deviation, the horizontal beds appear cuved relative to the borehole. Their interception angle with the borehole gradually decreases as the well lands horizontally into the reservoir.

Panel 1 of Figure 3(b) shows the *GR* (black) and *DEV* (red) curves for a horizontal well section of 120m, the value of *DEV* being nearly 90° and quite constant. The image from the *SV*-wave is displayed in panel 2, in a radial distance range about 23m on each side the well. Two major events are cearly identified in the image, crossing the well at about a 45° angle. Because the *SV*-wave refelctions are mostly from vertical reflectors, these events are interpreted as vertical fractures in the reservoir.

4. CONCLUSION

Single well acoustic reflection imaging has gained significant advances in recent years. The most important advance is the development of dipole-shear wave imaging technology. A particular advantage of the technology is its azimuthal sensitivity. With this advantage, the shear-wave reflection imaging has been applied to image bedding boundaries around borehole and detect reservoir fractures. Field data processing examples have demonstrated some important capabilities and applications of the borehole reflection imaging technology.

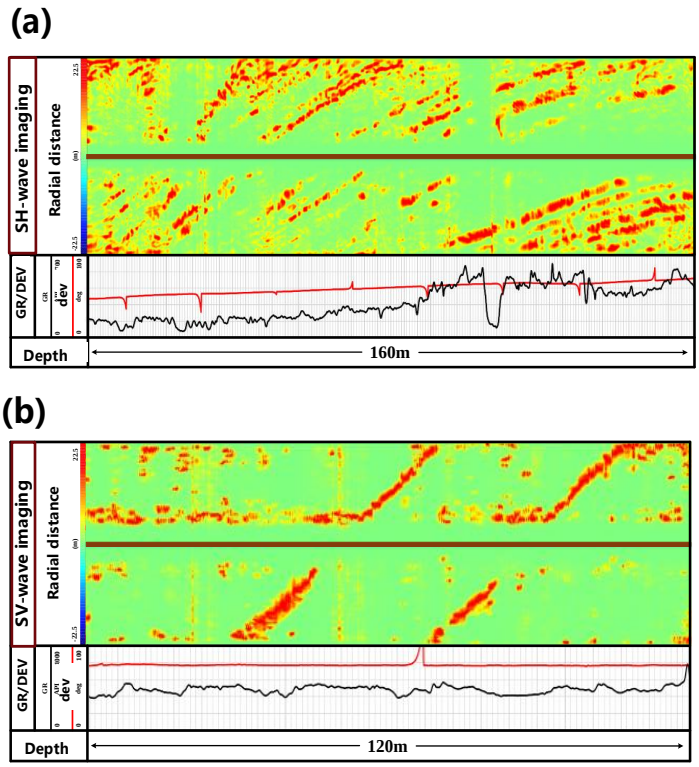

FIGURE 3: DIPOLE SHEAR-WAVE IMAGING FOR A DEVIATED (UPPER FIGURE, OBTAINED USING SH WAVE) AND A HORIZONTAL (LOWER FIGURE, OBTAINED USING SV WAVE) PART OF A WELL.

REFERENCES

[1] Hornby B. E., 1989, Imaging of near-borehole structure using full-waveform sonic data. Geophysics, 54, (6), 747-757.

[2] Fortin J., Rehbinder N., Staron P., 1991. Reflection imaging around a well with the EVA full-waveform tool. The Log Analyst, 32, (3), 271-278.

[3] Esmersoy C., Chang C., Kane M. R., 1997, Sonic Imaging: A Tool for High Resolution Reservoir Description, SEG 67th Annual Meeting, Extended Abstracts.

[4] Tang X. M., 2004, Imaging near borehole structure using directional acoustic wave measurement. Geophysics, 69, (6), 1378-1386.

[5] Bolshakov A. O., Patterson D. J., and Lan C., 2011, Deep fracture imaging around wellbore using dipole acoustic data, SPE Annual Technical Conference and Exhibition.

[6] Tang X. M., and Patterson D., 2009, Single-well S-wave imaging using multi component dipole acoustic log data. Geophysics, 74, (6), 211-223.

[7] Cao J. J., Tang X., Su Y., 2016. Radiation efficiency of a multipole acoustic source in a fluid-filled borehole. Chinese J. Geophy, 59(2): 757-766.

[8] Tang, X. M., Cao, J. J., and Wei, Z. T., 2014, Shear-wave radiation, reception, and reciprocity of a borehole dipole source: With application to modeling of shear-wave reflection survey, Geophysics, 79, (2), T43-T50.

© 2019 by ASME

[9] Tang, X. M., Zheng, Y. and Patterson, D., 2007, Processing array acoustic logging data to image near-borehole geologic structures: Geophysics, 72, (2), E87–E97.

[10] Tang, X. M., Cao, J., Li, Z., and Su, Y., 2016, Detecting a fluid-filled borehole using elastic waves from a remote borehole: J Acoust Soc Am. 2016 Aug;140(2): EL211. doi: 10.1121/1.4960143.

© 2019 by ASME